RAA 2014 Vol. **14** No. **3**, 249–274 doi: 10.1088/1674–4527/14/3/001
http://www.raa-journal.org *http://www.iop.org/journals/raa*

Research in Astronomy and Astrophysics

A possible precessing nozzle and the Lense-Thirring effect in blazar 3C 454.3

Shan-Jie Qian[1], S. Britzen[2], A. Witzel[2], T. P. Krichbaum[2], Heng-Qian Gan[1] and Long Gao[1]

[1] National Astronomical Observatories, Chinese Academy of Sciences, Beijing 100012, China; *rqsj@bao.ac.cn*
[2] Max-Planck Institüt für Radioastronomie, Auf dem Hügel 69, Bonn 53121, Germany

Received 2013 February 6; accepted 2013 October 22

Abstract The kinematics of superluminal components in blazar 3C 454.3 are studied. Nine components are included: superluminal knots R1, R2, R3, R4, A, B, C and D (from Britzen et al. 2013) and C4 (from Pauliny-Toth 1998). We find that their kinematics derived from VLBI observations can be consistently interpreted in terms of a jet precession scenario with a period of about 14.5 yr. We discuss the model fits of their trajectory, distance from the core and apparent velocity. We show that the bulk Lorentz factor (in the range 4 to 15) derived for these components does not have any dependence on the phase of the precession (or position angle for ejection). The Lense-Thirring effect is assumed to interpret the precession of the jet nozzle. The results obtained for blazar 3C 454.3 are only suggestive. They are not unique and have yet to be tested, but they might be useful for understanding the kinematics of superluminal components in blazars and for disentangling different mechanisms and factors.

Key words: radio continuum: galaxies — galaxies: jets — galaxies: kinematics — galaxies: individual (blazar 3C 454.3)

1 INTRODUCTION

3C 454.3 ($z = 0.859$) is one of the most prominent and well-studied blazars, which are flat-spectrum radio quasars with optically violent variations that show large, rapid, polarized outbursts. This blazar radiates across the entire electromagnetic spectrum from radio through optical and X-ray to TeV γ-rays. Very strong variability has been observed in all these wavebands with various timescales (hours/days to years). On the scale of parsecs, superluminal motion of components was detected by VLBI observations. Multi-wavelength observation campaigns combined with VLBI observations have been conducted in order to find the relationship between activities in different wavebands and relationship between outbursts and superluminal ejection that will give a better understanding their mechanisms that generate radiation and the location of sources that emit radio, optical and γ-rays in the jet. In recent years, coordinated observations in optical, X-ray and γ-ray combined with VLBI observations have provided important information and clarified some theoretical issues, e.g. the

relative location of regions that emit γ-ray and optical radiation in the jet. (see, e.g., Jorstad et al. 2007, 2010; Marscher 2008; Marscher & Jorstad 2011; Chatterjee et al. 2008).

Since 2005, blazar 3C 454.3 has shown remarkable flaring activity at all frequencies (e.g., Bonnoli et al. 2011; Bonning et al. 2009; Raiteri et al. 2008, 2011; Villata et al. 2006, 2007; Giommi et al. 2006; Pian et al. 2006; Tosti 2007; Vercellone et al. 2008, 2009, 2010, 2011; Vercellone 2011; Striani et al. 2010; Donnarumma et al. 2009; Abdo et al. 2009, 2010, 2011). In 2005, it was observed to undergo an unprecedented bright state from near-IR to hard X-ray frequencies (Raiteri et al. 2011); in May 2005 the source showed the strongest optical flare ever recorded and reached the optical magnitude $R = 12$ (Villata et al. 2006; Fuhrmann et al. 2006) which was followed by an mm-outburst and flux increase at high radio frequencies. In early 2006, a major mm-flare was observed, which was associated with a minor optical flare.

In γ-ray bands, 3C 454.3 was particularly active (e.g., Pacciani et al. 2010; Marscher et al. 2012; Raiteri et al. 2010; Finke & Dermer 2010). During four years (2007–2010) it exhibited more than one γ-ray flare per year, becoming the most active γ-blazar in the sky: On 2009 December 2–3, a super-γ-ray flare was observed, with brightness exceeding the Vela pulsar. On 2010 November 20 it reached a peak flux ($E > 100$ MeV) even exceeding that of the 2009 December 2–3 event, once more becoming the brightest γ-ray source in the sky.

By studying the evolution of the spectral energy distribution (SED) and correlation between the broadband emission (radio, optical and X-ray emission) and γ-ray flaring emission, understanding of the mechanism producing γ-rays has been greatly improved (Ghisellini et al. 2007; Vercellone et al. 2011; Tosti 2007).

Foschini et al. (2011) and Abdo et al. (2011) indicated that the extremely fast variability on a timescale of about 3–6 hr favors γ-ray emission originating from a compact region smaller than the scale of a parsec, or in the compact core observed with VLBI.

3C 454.3 has been monitored with VLBI since Pauliny-Toth et al. (1987) and Pauliny-Toth (1998) detected some peculiar properties on the scale of parsecs: (1) superluminal brightening of a stationary structure; (2) co-existence of a stationary component and superluminally moving components; (3) apparent acceleration of knots; (4) apparent extreme curvature in the trajectory. These features could be understood in terms of hydrodynamical simulations and the theory of relativistic flows (e.g. Daly & Marscher 1988; Agudo et al. 2001; Gomez et al. 1997).

Recently, Britzen et al. (2013) investigated the structure observed at 15 GHz with VLBI during a very long period of about 16 yr (1995.6–2011.5) and studied the correlations between flaring properties in radio and optical bands and the structure of the source as observed by VLBI. They found for the first time that during the period (1996–2010) a superluminally expanding ring dominated the structure on the scale of parsecs for 14 yr. They also suggested that this phenomenon might be related to the convergent motion of the superluminal components and associated relativistic plasma. Another interesting property was the change in the pattern of flux variability: before 1995 major radio outbursts were followed by smaller flares, but after 1995 faster radio flaring activity started. This change in the pattern of radio variability might be related to a change in the kinematics of components forming the inner jet (Britzen et al. 2013).

In 3C 454.3, the range of ejection position angle of the superluminal knots was observed to be very large, about 80° (position angle is $\sim -30^\circ$ for knot R1 and position angle is $\sim -110^\circ$ for knot R3). This phenomenon of swing or wobbling in the jet has been observed in other AGN sources (especially blazars) but its physical origin is poorly understood and under debate (Bach et al. 2005; Agudo et al. 2001; Agudo 2009; Agudo et al. 2007, 2011; Britzen et al. 2010; Kudryavtseva et al. 2011; Kudryavtseva & Pyatunina 2006; Qian et al. 2007; Qian 2011; Savolainen et al. 2006). The problem is whether these swings are regular (due to precession) or irregular (due to, e.g., instabilities). In most cases the kinematics of superluminal components are very complex and it is very

difficult to disentangle the effects of different mechanisms and different factors within one mechanism. Qian (2011, 2012) attempted to study and disentangle the effects of jet precession in blazar 3C 279. In this paper we will investigate whether the swing of the position angle for ejection that was observed in 3C 454.3 could be due to precession in the axis of the jet. We know that phenomena that occur on the scale of parsecs in 3C 454.3 are very complex, and different mechanisms could play various roles, thus precession of the jet could only be one of the factors that affect features on the scale of parsecs. In fact, only for part of the superluminal components can the precession scenario be applied to consistently interpret their kinematics.

Valtonen & Wiik (2012) and Katz (1997) have shown that for interpreting the periodic behavior observed in the optical light curves of OJ 287, a binary black-hole scenario would be a plausible mechanism in which the precession and nodding of the optical jet are factors responsible for the motion. Valtonen & Wiik (2012) also applied this mechanism to explain the long-term swing of both optical and radio jets. Thus effects of jet precession could be involved in the swing of the jet's position angle in OJ 287 on long-term time scales (at least as one of the factors).

Very recently, based on 7-mm VLBI observations, Agudo et al. (2012) found swings in the position angle of the jet in blazar OJ 287 on short timescales (~ 2 yr, with an amplitude of $\lesssim 40^\circ$) and a sudden jump ($> 100^\circ$) in the position angle of its jet during 2004–2005. They argued that the swing in the position angle of the jet could be erratic. However, Tateyama & Kingham (2004) showed that during the time range of 1995–2004, the swing in the jet's position angle observed at 3.5 cm could be interpreted in terms of a precessing nozzle model with a period of $\sim$12 yr. This regular swing in the jet was supported by observations during the period 1995–2005 made by Moór et al. (2011), but this behavior was discontinued by a jump in the position angle of the jet detected by Agudo et al. (2012) at 7 mm. Similarly, Qian (2011, 2012, 2013) showed that the kinematics of sixteen superluminal components in blazar 3C 279 (during the period of $\sim$1980–2007) could be consistently interpreted in terms of a model with a precessing jet nozzle with a period of $\sim$25 yr, taking into account curvatures in trajectories of the components. However, Lu et al. (2013) demonstrated that the orientation of the jet in 3C 279 sharply varied after $\sim$2007–2008 from $\sim -130^\circ$ to $\sim +130^\circ$ and this unexpected process seems to "temporarily break off" its regular (precession) behavior.

Therefore, wobbling in the jet observed in both blazars 3C 279 and OJ 287 seems to show that they are not a single phenomenon and a few mechanisms (processes) or constituents may be involved in their production (as suggested by Qian 2011, 2012, 2013). These mechanisms might include those causing erratic swings on short timescales (with timescales of $\sim$2 yr and amplitudes of $\lesssim 40^\circ$), regular swings on longer timescales (e.g. with timescales of $\sim$10–25 yr) and a sharp jump in the orientation of the jet of $\sim 100^\circ$.

In this paper, we will discuss the possibility that the kinematics of the superluminal components in blazar 3C 454.3 could be interpreted in terms of a scenario with a precessing jet nozzle that leads to curvatures in the trajectory. We will adopt the concordant cosmological model (ΛCDM model) with $\Omega_m = 0.3$, $\Omega_\Lambda = 0.7$ and Hubble constant $H_0 = 70$ km s^{-1} Mpc^{-1} (Spergel et al. 2003). Thus for 3C 454.3, $z = 0.859$, its luminosity distance is $D_\mathrm{l} = 5.483$ Gpc (Hogg 1999; Pen 1999) and angular diameter distance $D_\mathrm{a} = 1.586$ Gpc. Angular scale of 1 mas = 7.69 pc and proper motion of 1 mas yr^{-1} are equivalent to an apparent velocity of 46.58c.

The data used were collected from Britzen et al. (2013) (knots R1, R2, R3, R4, A, B, C and D), and from Pauliny-Toth et al. (1987) and Pauliny-Toth (1998) (knot C4). Errors in position shown in the figures were computed from observational errors in position angle and distance from the core. Hereafter, the distance from the core will be called core distance.

The plan of the paper is: Section 2 gives the formalism of the model; Section 3 describes the fitting of the kinematics of the knots; Section 4 gives a summary of the results; Section 5 discusses the mechanisms causing precession of the jet nozzle; Section 6 gives a conclusion.

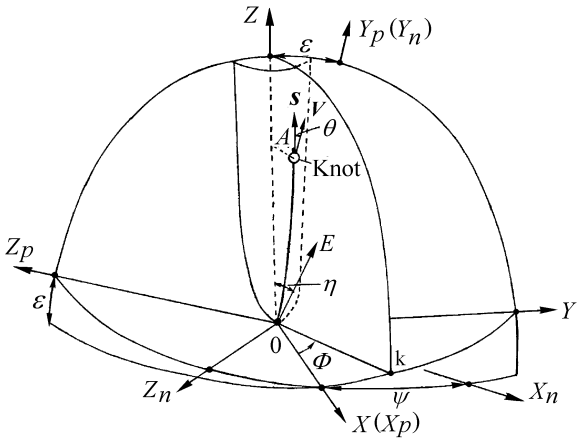

Fig. 1 The geometry of the precession model, adopted from Qian (2011). The Z-axis, which is taken to be the axis of precession, is defined by parameters (ϵ, ψ); the Y_p-axis indicates the direction toward the observer; the position of a knot is defined by parameters (A, Φ): $A(Z)$ is the amplitude function and Φ is the azimuthal angle; plane (X_n, Z_n) represents the plane of the sky; $\boldsymbol{S}$ denotes the velocity of the knot.

2 FORMALISM OF THE MODEL

We will apply the formalism and geometry of the precession model which has been described in detail in the previous paper by Qian (2011, also see Qian et al. 2009, 1991). The geometry is shown in Figure 1 in which some explanations are given. Here we only recall the expressions describing the amplitude function and the precession phase of the knots. (Coordinates and amplitude (A) are measured in units of mas.)

In order to study the possible precession of the jet nozzle in blazar 3C 454.3, we would have to choose an appropriate set of model parameters and functions to describe the amplitude and phase of the knots, defining their trajectories and velocities. This mainly includes the direction of the precession axis (ϵ, ψ), the amplitude function $A(Z)$ and the period of precession $T_{\rm p}$. These parameters cannot be determined theoretically and we have chosen these parameters through trial fittings of the model to as many of the kinematics of superluminal components as possible. Hereafter, fitting of the data to our model will simply be called fitting.

The position of a knot is described by cylindrical coordinates (Z, A, Φ), where Z is the distance from the core along the axis of precession, A is the amplitude of the path and Φ is the azimuthal angle.

– The precession axis of the jet is defined by two parameters (ϵ, ψ); we take $\epsilon = 2.88^\circ$ and $\psi = -17.91^\circ$.
– Amplitude (A) as a function of Z is taken as

$$A(Z)(\mathrm{mas}) = 3.34{\times}\sin\left(\frac{\pi Z}{Z_*}\right), \tag{1}$$

with Z_*=240 mas; only the rising part of the sine function is applied.

– The azimuthal angle Φ is defined by

$$\Phi(Z,t) = \phi_0 + \phi(t) + R_\phi \times Z, \tag{2}$$

where ϕ_0=3.783 rad is an arbitrarily selected constant and in the following ϕ(t) is defined as the (initial) precession phase of the knot, given by

$$\phi(t)(\mathrm{rad}) = 0.8132 + 0.4335(t - 2009.60), \tag{3}$$

where t is the ejection time (in units of years). Period of precession $T_\mathrm{p} = 14.49$ yr. R_ϕ is defined as a rotation rate (rad/mas) after ejection. This form of the amplitude function shows a slightly collimated track (for all knots $Z < 120$ mas included in the fitting) and rotation of trajectory for some knots when $R_\phi \neq 0$.

– The formulas for viewing angle θ, apparent transverse velocity β_a, Doppler factor δ and elapsed time T are given as follows.

$$\theta = \arccos[\cos\epsilon(\cos\Delta + \sin\epsilon\tan\Delta_p)]\,, \tag{4}$$

$$\delta = \frac{1}{\Gamma(1-\beta\cos\theta)}\,, \tag{5}$$

$$\beta_a = \frac{\beta\sin\theta}{1-\beta\cos\theta}\,, \tag{6}$$

$$T = \int_0^Z \frac{1+z}{\Gamma\delta v\cos\Delta_s} dZ\,, \tag{7}$$

where z is the redshift, the expressions for Δ, Δ_p and Δ_s are given in Qian (2011; 1991). δ is the Doppler factor of a knot, Δ is the angle between the spatial velocity vector and Z-axis; Δ_p is the projection of Δ on the (Y, Z) plane; and Δ_s is the angle between the velocity vector of a knot and the direction toward the observer.

Figure 2 shows a VLBI map adopted from Britzen et al. (2013) in which the superluminal components are designated (R1, R2, R3, R4, A and C). Figure 3 shows the distribution of trajectories for knots R1, R2, R3, R4, C4, A, B, C and D which are investigated in this paper.

3 FITTING A MODEL DESCRIBING THE KINEMATICS OF THE KNOTS

In the following we describe in detail the fitting results for each individual superluminal knot. The fitting techniques are similar to those described in Qian (2011), including the fitting of the ejection time (epoch, t_0); trajectory (X_n, Z_n) [1]; core distance (r_n) and apparent velocity (β_a). Bulk Lorentz factor (Γ) has been derived. In this paper, we would also like to include other factors (for example, rotation of trajectory) in addition to precession of the jet.

Before presenting the fitting results for individual superluminal knots, we would like to mention two points about our fitting methods. Firstly, since we are interested in possible precession of the jet nozzle, we would mainly fit the inner parts of the jet (values of X_n less than about 1.5–2 mas). Secondly, as shown by Britzen et al. (2013) knots R1 to R4 were observed to be distributed along an arc-like structure at the boundary between the surrounding interstellar medium and the source, and their tracks converged toward the position (X_n ∼3 mas, $Z_n \sim -1$ mas). Thus their trajectory significantly changed in these regions: beyond X_n ∼1.8 mas for knot R1, ~ 2.5 mas for knots R2 and R4, and ~ 3 mas for knot R3 (see Figs. 4, 7, 9 and 11 (left) below). The kinematic behavior of

[1] X_n and Z_n are defined as relative right ascension (west) and relative declination (north), respectively.

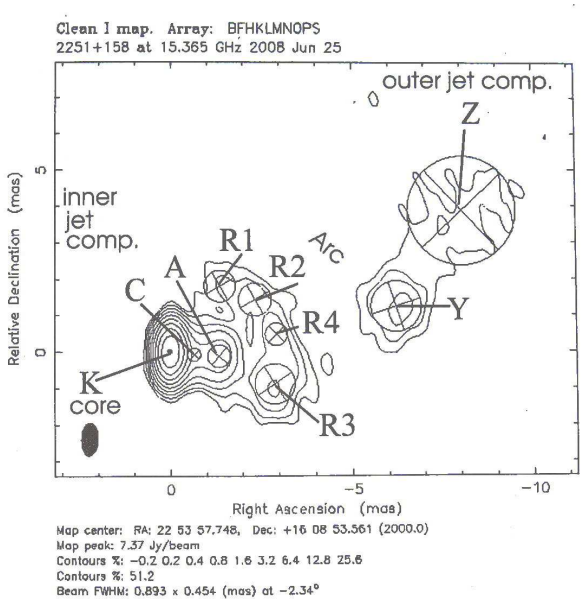

Fig. 2 VLBI map of 3C 454.3 at epoch 2008 June 25 at 15 GHz, adopted from Britzen et al. (2013; by courtesy of S. Britzen). The designation of the components (A, C, R1–R4, Y and Z) is shown.

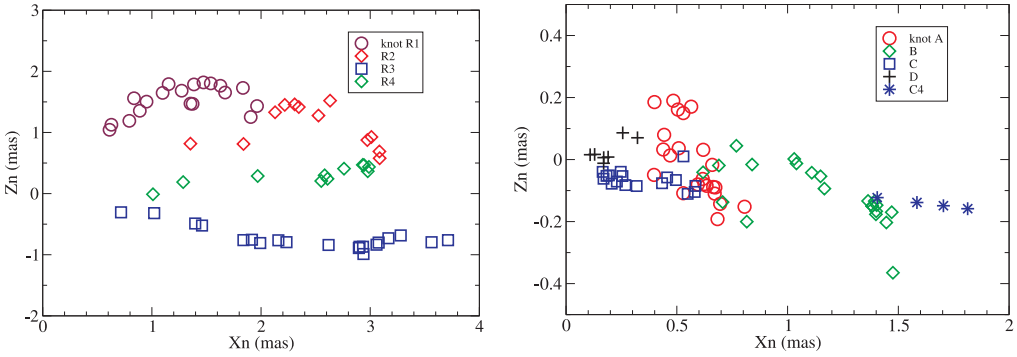

Fig. 3 The distribution of the observed trajectory for superluminal components in 3C 454.3. *Left panel*: knots R1, R2, R3 and R4; *right panel*: knots C4, A, B, C and D.

the knots and associated plasma flows may be very complex in these regions and seems very difficult to describe. Thus in the following we will not fit the kinematics of these parts of the trajectories for knots R1, R2, R3 and R4. Fortunately, the lack of VLBI observations and results from fitting for these parts of their trajectories does not affect our study of precession in the jet nozzle near the core.

The fitting results are summarized in Table 1, including ejection time t_0, precession phase ϕ, rotation rate R_ϕ, bulk Lorentz factor Γ, initial position angle (IPA) and initial viewing angle (IVA) for nine superluminal components (C4, R1, R2, R3, R4, A, B, C and D).

Table 1 Model parameters for nine superluminal components: ejection time t_0, precession phase ϕ, rotation rate R_ϕ, bulk Lorentz factor Γ, initial position angle (IPA) and initial viewing angle (IVA).

Knot	t_0	ϕ (rad)	R_ϕ (rad/mas)	Γ	IPA (°)	IVA (°)
C4	1978.88	0.06	0.0	14.2	–95.6	4.9
R2	1982.88	1.80	–0.02	6.2	–48.6	4.9
A	1985.36	2.87	–0.38	3.5	–23.0	3.3
R1	1987.20	3.67	0.0	10.7	–8.8	1.1
B	1988.45	4.21	0.02	10.0	–119.9	0.5
R3	1992.00	5.75	0.0	9.5	–111.2	4.0
R4	1995.31	0.90	–0.02	11.0	–72.9	5.4
C	2007.41	6.15	0.0	7.1	–100.7	4.6
D	2009.30	0.68	0.0	6.5	–75.2	5.4

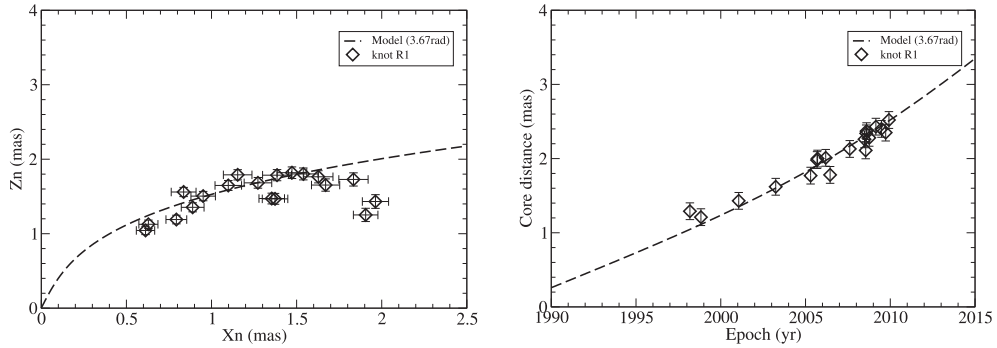

Fig. 4 Fitting to the trajectory and core distance of knot R1. Ejection epoch $t_0 = 1987.20$.

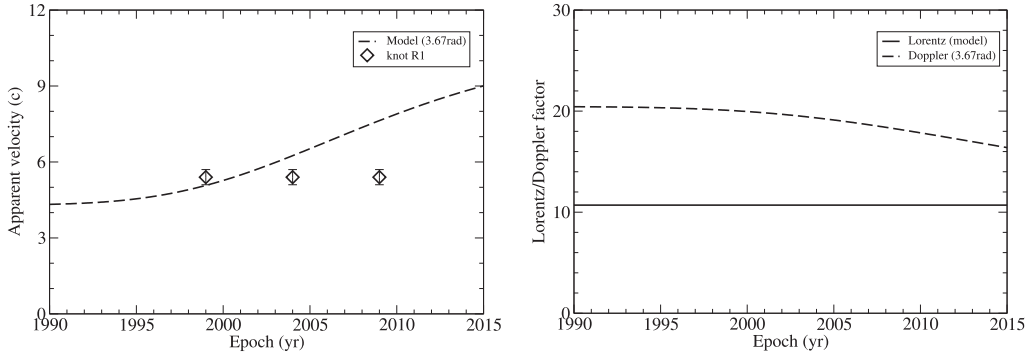

Fig. 5 Fitting to the apparent velocity (*left panel*) and the Lorentz/Doppler factor derived from the model (*right panel*) for knot R1. After 2005, the apparent velocity given by our model is slightly larger than that given by Britzen et al. (2013), which might be due to our model applying non-ballistic motion.

3.1 Knot R1

Knot R1 is the northernmost component observed with an ejection position angle of $\sim -9°$. The fitting results are shown in Figures 4 and 5.

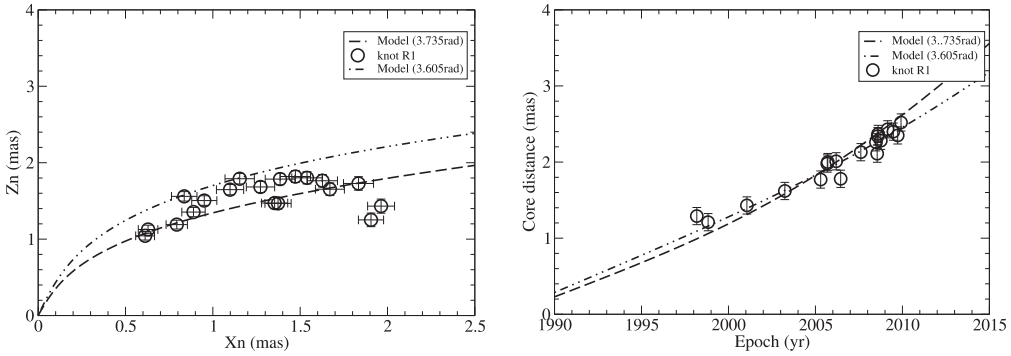

Fig. 6 Fitting to the trajectory and core distance for ejection time $t_0 = 1987.35$ and 1987.05, which differ from those in Fig. 4 by $\pm$0.15 yr. The bulk Lorentz factors used for fitting the core distance (*right*) are 11.1 ($t_0 = 1987.35$) and 10.3 ($t_0 = 1987.05$), respectively.

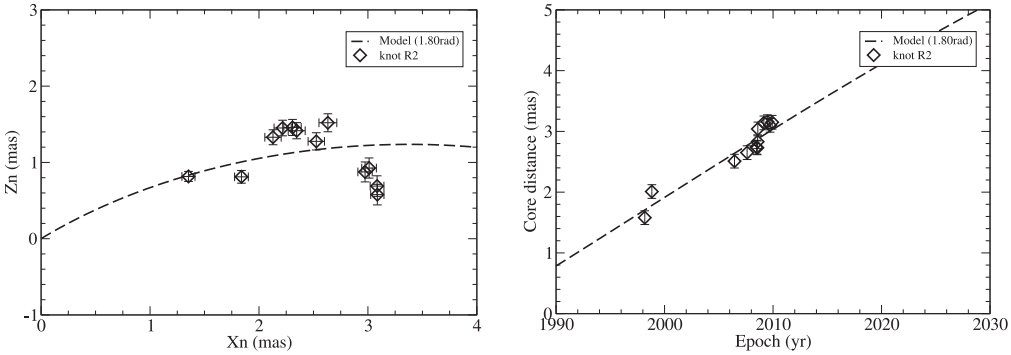

Fig. 7 Fitting the model to the trajectory and core distance for knot R2.

As shown in Figure 4, the trajectory within $X_n \simeq$1.7 mas and the core distance are both well fitted. The apparent velocity given by the fitting (Fig. 5 (left)) is very consistent with the value given by Britzen et al. (2013) before 2005. After 2005, the apparent velocity given by our model is a bit larger than that derived by Britzen et al. (2013). This might be due to the application of different models: in Britzen et al. (2013) a velocity for ballistic motion (along a straight line) was estimated but in our case non-ballistic motion was studied. However, both can fit the core distance vs time well.

In addition, in Figure 6 (left) two trajectories from the fitting are given for ejection epochs $t_0 =$ 1987.05 and 1987.35, corresponding to precession phases $\phi = 3.605$ and 3.735 rad, respectively. In comparison with Figure 4, it can be seen that for $t_0 = 1987.05$ and 1987.35 the model curves have already discernibly deviated from the observed positions, so the uncertainty in the fitting of ejection time t_0 might be roughly estimated as $<$0.15 yr. In Figure 6 (right) the two model curves show the fits to the distance from the core with Lorentz factors of 11.1 (for $t_0 = 1987.35$) and 10.3 (for $t_0 = 1987.05$), which differ from that for $t_0 = 1987.20$ ($\Gamma = 10.7$; Fig. 4 (right)) by ± 0.4.

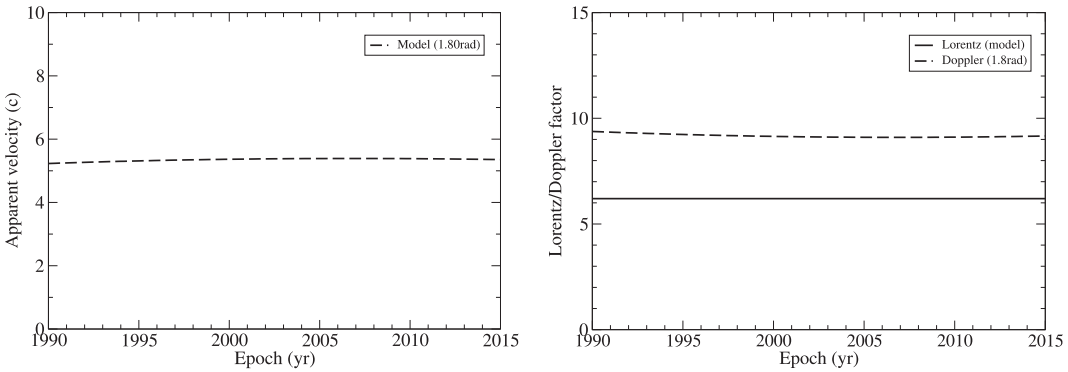

Fig. 8 Fitting of the apparent velocity and the Lorentz/Doppler factor derived from the model for knot R2.

3.2 Knot R2

The fitting results are shown in Figures 7 and 8. The fitting of its apparent path within $X_n \simeq 2.5$ mas is only marginal, but the modeled trajectory could approximately describe its motion derived by the model with the chosen ejection time and corresponding precession phase. The core distance is fitted reasonably well.

3.3 Knot R3

Knot R3 is the southernmost component observed with its ejection position angle of $\sim -110°$. The fitting of its trajectory to the model is shown in Figure 9 (left) and part of it within $X_n < 2.8$ mas is fitted well. The fitting of its core distance and apparent velocity is also good (Figs. 9 (right) and 10 (left)). The good fitting of the kinematics for both knots R1 and R3 may be meaningful. Considering that knot R3 was ejected later than knot R1 by about 5 yr (corresponding to a third of its period of precession) and their position angle for ejection differs by about $100°$ (R1 is the northernmost component and R3 is the southernmost component, see Fig. 3 (left)), this may indicate that the direction of the precession axis for the jet, the amplitude function and the period of precession have been appropriately chosen for our precession model. Good fittings for more knots ejected at different epochs (for example, knots A, C4, C and D, below) would provide further support.

In addition, in Figure 11 two trajectories described by the model are given for ejection times $t_0 = 1991.85$ and 1992.15, corresponding to precession phases $\phi = 5.707$ and 5.793 rad, respectively. It can be seen that the trajectories for $t_0 = 1991.85$ and 1992.15 have already discernibly deviated from the observed positions, so the uncertainty in the fitting of the ejection epoch for knot R3 may be roughly estimated as < 0.15 yr, similar to knot R1.

3.4 Knot R4

The fitting results are shown in Figures 12 and 13. For knot R2, the fitting to the inner part of its trajectory within $X_n < 2.5$ mas is only marginal (as for knot R2), because only three data points are presented. This fitting might only have shown a trend in its motion (within $X_n \lesssim 2$ mas), which could be roughly described by the precession model. Its core distance is fitted well. There is no observed apparent velocity available to be compared with.

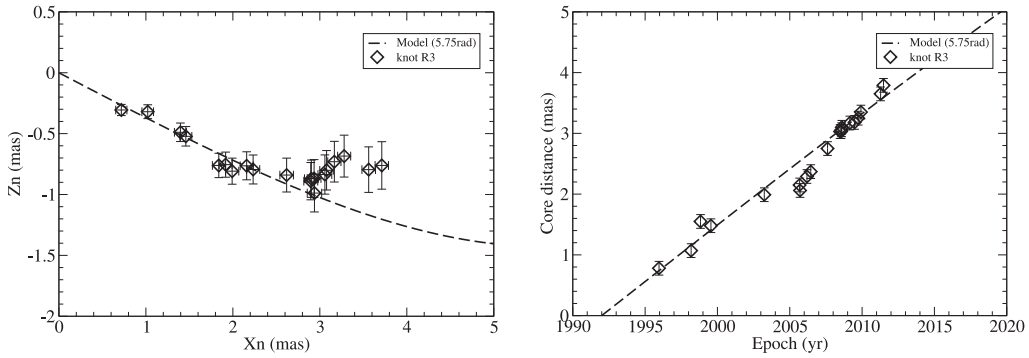

Fig. 9 Fitting of the trajectory and the core distance for knot R3. Note: beyond $X_n = 3$ mas, the trajectory is obviously curved upward and this may indicate convergence of its motion. See Fig. 26 (left) below.

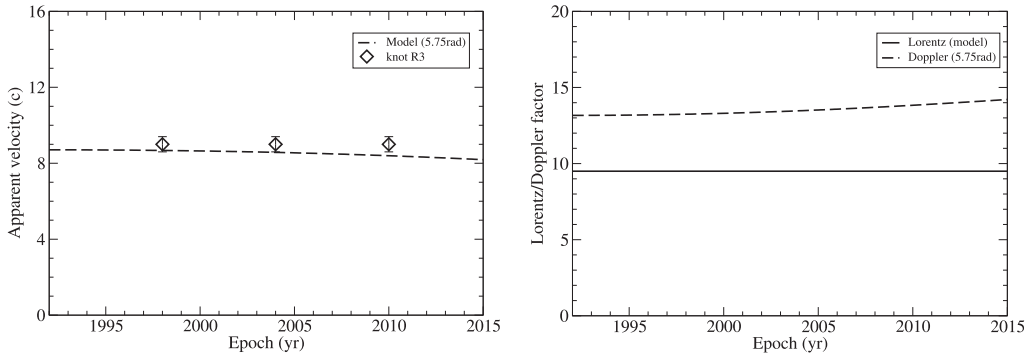

Fig. 10 Fitting of the apparent velocity and the Lorentz/Doppler factor derived from the model for knot R3. The apparent velocity derived from our fitting is very consistent with the value (9.0±0.4) given by Britzen et al. (2013).

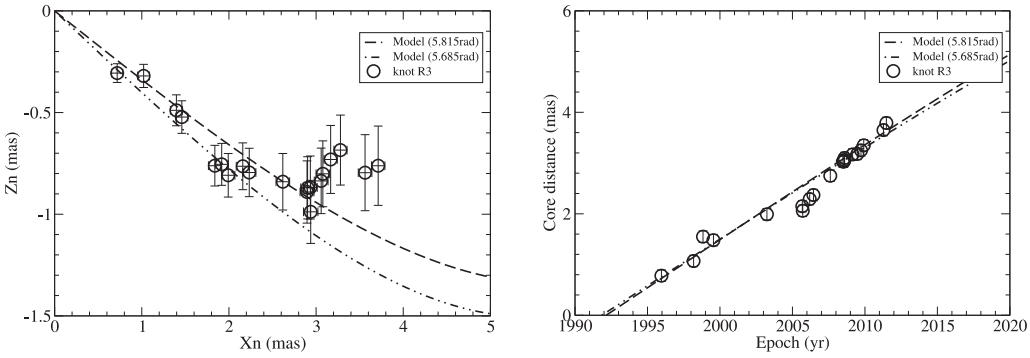

Fig. 11 Fitting of the trajectory (*left*) and core distance (*right*) for ejection time $t_0 = 1992.15$ (precession phase $\phi = 5.815$ rad) and 1991.85 ($\phi = 5.685$ rad). It can be seen that the trajectories discernibly deviate from the observed positions, indicating uncertainty in the fitting of the ejection time for <0.15 yr. The Lorentz factors used for the fitting of the core distance are 9.5 and 9.6, respectively.

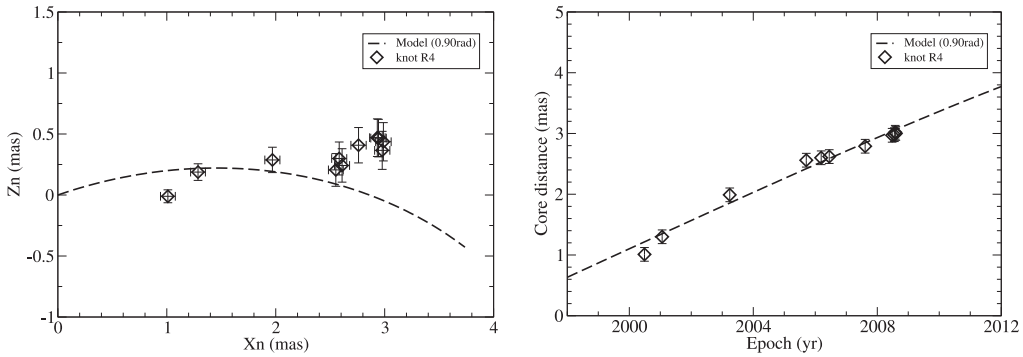

Fig. 12 Fitting of the trajectory and core distance for knot R4.

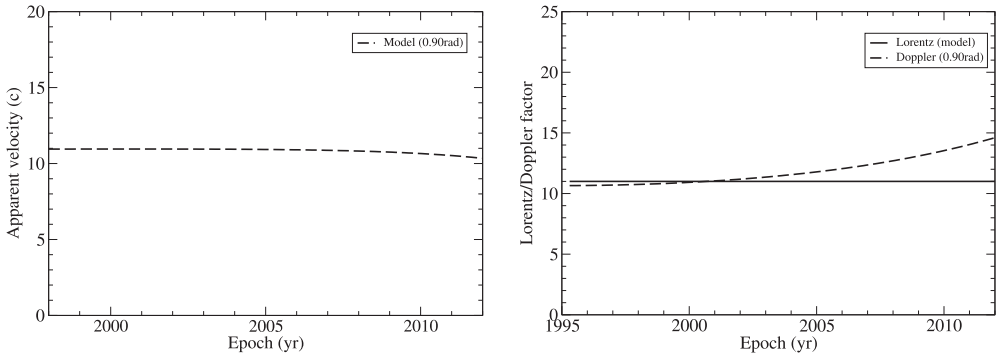

Fig. 13 Fitting to the apparent velocity and the Lorentz/Doppler factor derived from the model for knot R4.

3.5 Knot A

The fitting results are shown in Figures 14 and 15. The kinematics of knot A seems difficult to fit: the observed trajectory is very curved and the core distance of the initial portion of its trajectory appears almost constant (Fig. 14 (right)), which leads to its ejection time being difficult to determine. Britzen et al. (2013) divided it into two components (before and after 2005) and determined their apparent velocity, respectively. For consistency we would alternatively make a tentative fit to the kinematics of knot A as one component within the precession scenario. In this case a large rotation rate R_ϕ has been introduced, which might imply that knot A moved along a helical trajectory. Taking into account the rather large amplitude in the wandering motion of the measured positions between consecutive epochs, the fits of the trajectory and distance from the core (Fig. 14 (left)) might be regarded as acceptable. The apparent velocity derived for the period (2007–2011) is consistent with that (2.2 ± 0.5) given by Britzen et al. (2013).

3.6 Knot B

The fitting results are shown in Figures 16 and 17. Similar to knot A, the kinematics of knot B is also difficult to fit. This is because the core distance of the initial portion of its trajectory was observed to be almost constant (Fig. 16 (left)). Thus it is difficult to determine its ejection time. Britzen et al. (2013) divided knot B into two components and separately fitted their kinematics. Here we have

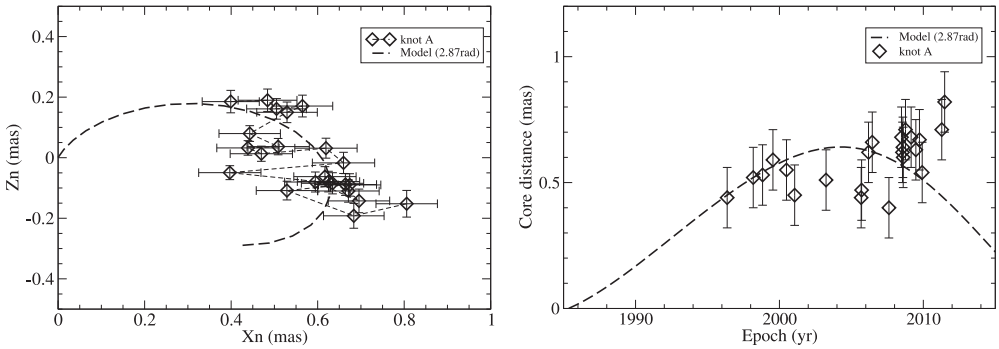

Fig. 14 Fittings to the trajectory and distance from the core for knot A.

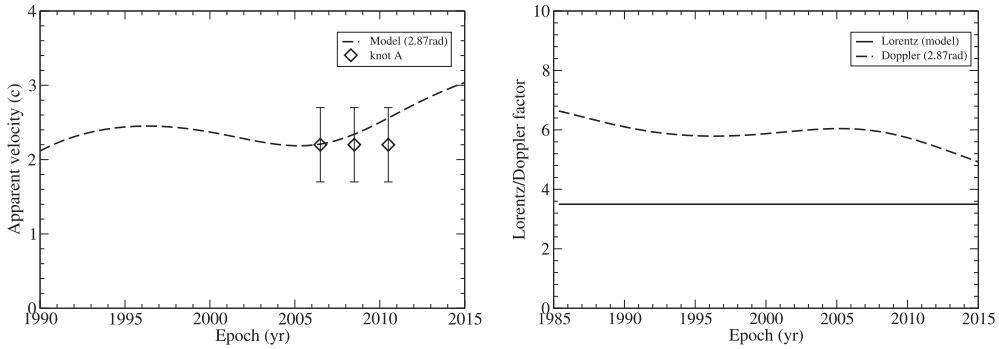

Fig. 15 Fitting of the apparent velocity and the Lorentz/Doppler factor derived from the model for knot A.

made a tentative fit to the kinematics of knot B as one component in terms of our precession model. In this case a small rotation rate R_ϕ has been introduced.

In Figures 16 and 17 the fitting results for its trajectory, core distance and apparent velocity are shown. The fit to the trajectory within X_n <1.3 mas seems acceptable. The fit to the core distance before epoch 2004 is only marginal, implying there is a bit larger bulk Lorentz factor during this period, but the apparent velocity derived for the period (2006–2011) is very consistent with that (5.5±0.5) given by Britzen et al. (2013).

3.7 Knot C4

We assume that the ejection time $t_0 = 1978.88$, because C4, detected by Pauliny-Toth et al. (1987), was ejected before the outburst (1980–1981) causing the "superluminal brightening." Pauliny-Toth (1998) gave $\beta_a = 16.1 \pm 2.7$.

As shown in Figures 18 and 19, the trajectory, core distance and apparent velocity are all fitted well. In this case, the modeled Doppler factor δ is smaller than the bulk Lorentz factor Γ (Fig. 19 (right)).

We notice that knot C4 was ejected at position angle $-95°$ (Pauliny-Toth 1998), close to that of knot R3 ($-110°$), but their ejection times differed by about 13 yr, corresponding to precession phase differing by about 5.7 rad; C4 was ejected earlier than R3 by 13 yr. Thus the good fitting of the kinematics of knot C4 might be helpful for the interpretation of the phenomenon observed by VLBI in 3C 454.3 in terms of the precession model.

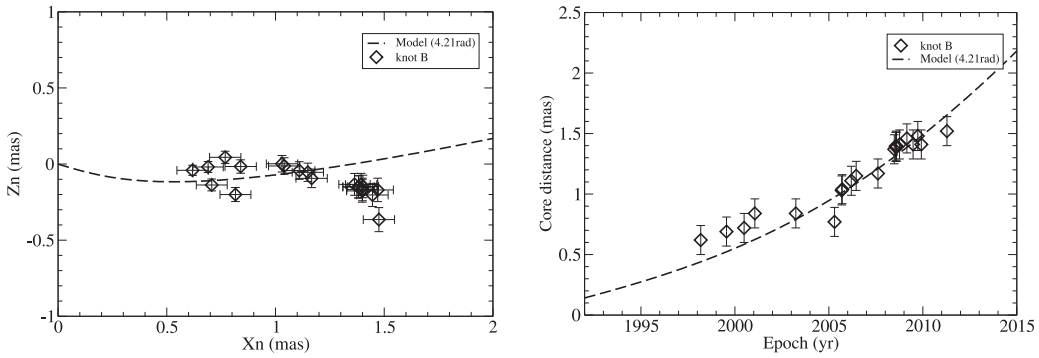

Fig. 16 Fitting to the trajectory and core distance of knot B.

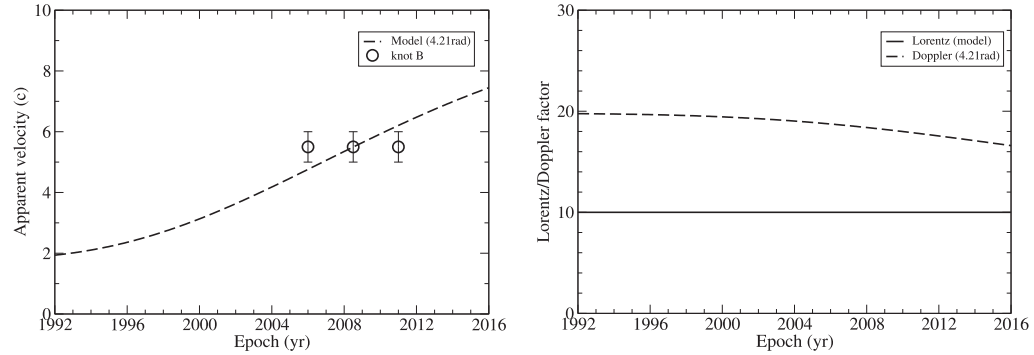

Fig. 17 Model fit of the apparent velocity (after epoch 2004) and the Lorentz/Doppler factor derived from the model for knot B. The apparent velocity from the model fit is very consistent with the value given by Britzen et al. (2013).

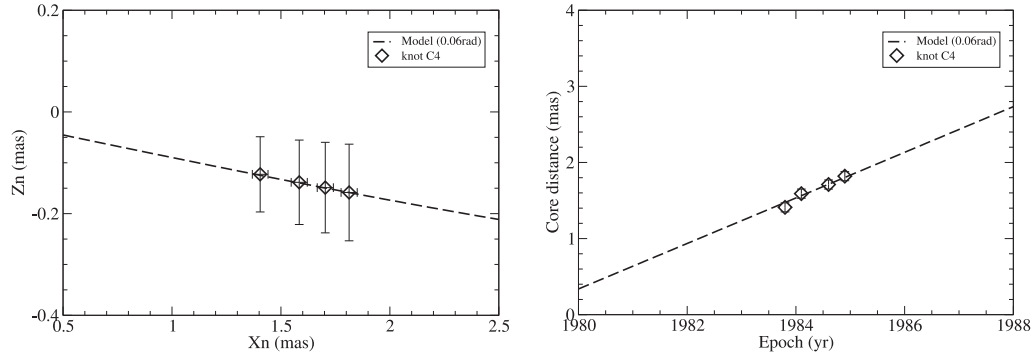

Fig. 18 Model fit to the trajectory and core distance for knot C4.

3.8 Knot C

The fitting results are shown in Figures 20 and 21. Knot C was ejected at 2007.4, later than knot R3 by about 15 yr (i.e. about one period of precession). The good fit to its trajectory, core distance and apparent velocity (shown in Figs. 20 and 21) is significant, because it may indicate that the proposed

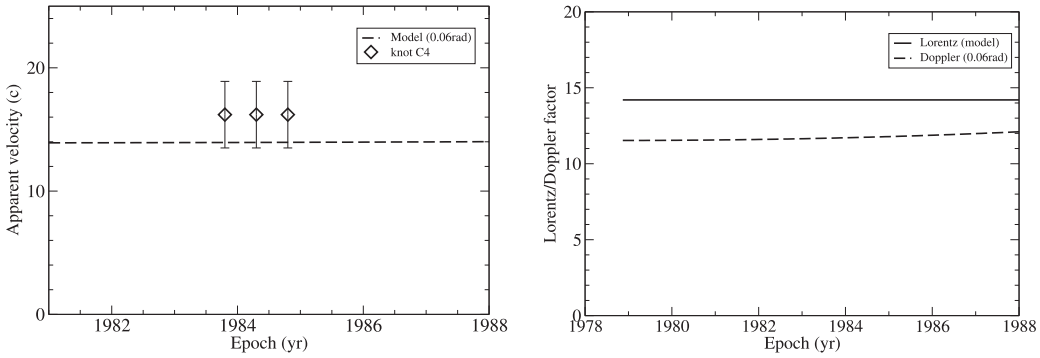

Fig. 19 Fitting for the apparent velocity and the Lorentz/Doppler factor derived from the model for knot C4. The observed apparent velocity (Pauliny-Toth et al. 1987) is fitted well, indicating that knot C4 moved ballistically during the period of six years (1979–1985) within a core distance of 2 mas.

precession model is applicable, at least for some of the superluminal knots in 3C 454.3. We notice that the motion of knot C is apparently ballistic, quite different from the curved trajectory of knots R1 and R3, but they are all produced from the same spatial trajectory described by the amplitude function (Eq. (1)). This demonstrates that the period of precession has been chosen properly. We would like to emphasize that combined with the good fitting of the kinematics for knot C4, the interval that our fitting covers is about two cycles (from $\sim$1979 to 2007), see Figure 27 (right) below.

In addition, two trajectories described by the model are given in Figure 22 for ejection times $t_0 = 2007.71$ and 2007.11, corresponding to precession phases $\phi = 6.277$ rad and 6.017 rad, respectively. It can be seen that the two trajectories described by the model have discernibly deviated from the observed positions and thus the uncertainty in the fitting of the ejection time of knot C may be estimated as $<$0.30 yr (in comparison with the fitting of the trajectory in Fig. 20 (left)).

The derived ejection time t_0 (2007.41) and ejection position angle ($-100.7°$) are very consistent with the values given by Britzen et al. (2013): $t_0 \sim 2007.3$, and the average position angle ($-102.3° \pm 5.4°$) within a core distance of 0.6 mas.

3.9 Knot D

The fitting results are shown in Figures 23 and 24. We assumed the ejection time is 2009.30, which is different from that (2009.6) given by Britzen et al. (2013). This is because in our precession model that only applies to $t_0 = 2009.30$ (corresponding to precession phase $\phi = 0.683$ rad), the trajectory of knot D could be fitted, as shown in Figure 23 (left). The fitting of the core distance is good enough to derive an apparent speed of $\sim$6 before $\sim$2000.8. The model fit also showed that after 2010.8, knot D could have an apparent acceleration (see Fig. 25).

Surprisingly, we found that the component K09 detected by Jorstad et al. (2012) at 43 GHz and knot D detected by Britzen et al. (2013) at 15 GHz may be identified as the same component and our model could give a good fit for the initial part of the core distance of K09 observed at 43 GHz before 2011 (as shown in Fig. 25), which is fully consistent with the fitting results at 15 GHz. Moreover, Figure 25 also shows an apparent acceleration after 2011. This may also verify our discovery that in the fitting by applying a precession model, we should use the "initial" trajectory (within a core

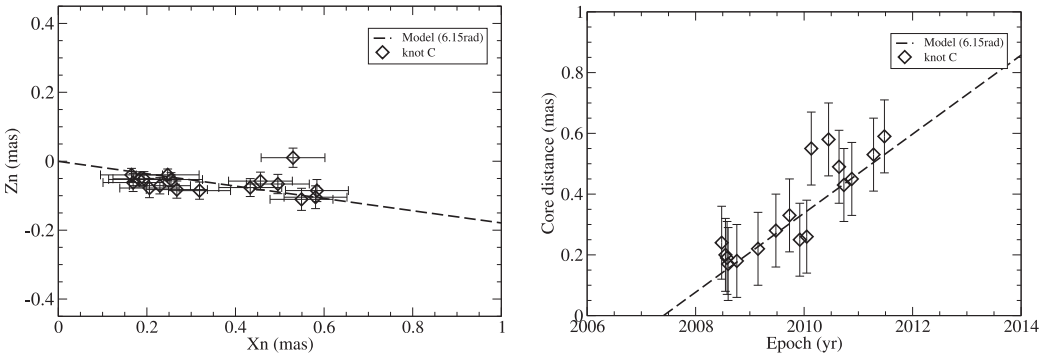

Fig. 20 Fittings of the trajectory and core distance for knot C.

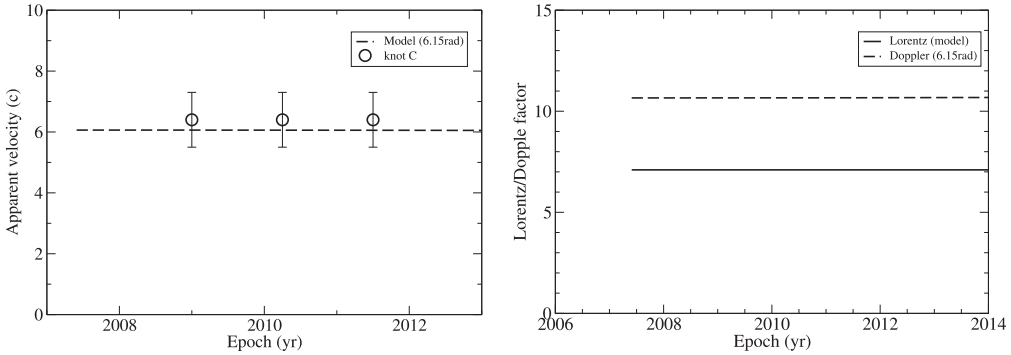

Fig. 21 Fitting for the apparent velocity and the bulk Lorentz/Doppler factor derived from the model for knot C. The apparent velocity of the model is very consistent with the value (6.4 ± 0.9) given by Britzen et al. (2013).

distance of $\sim$0.2–0.4 mas), which is unexpectedly consistent with the fitting techniques used for blazar 3C 279 (Qian 2011, 2012, 2013).

The derived ejection position angle ($-75.2°$) is very consistent with the observed average position angle ($83.3°\pm7.4°$) within a core distance of 0.3 mas (derived from the data given by Britzen et al. 2013).

4 SUMMARY OF RESULTS

We briefly summarize the results that we have obtained.

(1) In the above, we have fitted the kinematics (trajectory, core distance and apparent velocity) of nine superluminal components with the model describing blazar 3C 454.3. The fitting is based on precession of the jet nozzle with a period of about 14.5 yr (strictly speaking, a quasi-period). We find that, on the whole, their kinematics (trajectory, core distance and apparent velocity) can be consistently explained in terms of the proposed precession scenario (see Figs. 4–24). The fittings for knots C4, R1, R3, A, C and D seem good enough to recognize the period of precession, but the fittings for knots R2, R3 and B are only marginal, just showing trends in their motion. The ejection time of the nine knots spans nearly two precession cycles ($\sim$30 yr) and the swings in the ejection position angle of the knots were observed to be in the range of $\sim100°$. This might indicate that the precession model is meaningful.

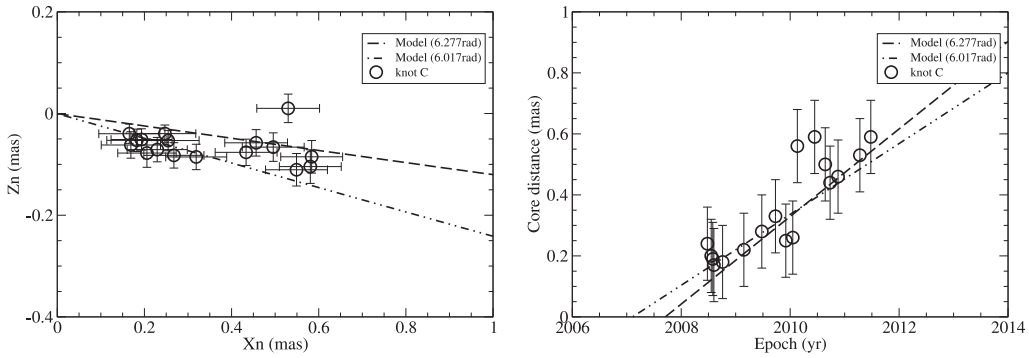

Fig. 22 Fitting of the trajectory (*left*) and core distance (*right*) of knot C for ejection times $t_0 = 2007.71$ ($\phi = 6.277$ rad) and 2007.11 ($\phi = 6.017$ rad) with Lorentz factors $\Gamma = 7.5$ and 6.7, respectively.

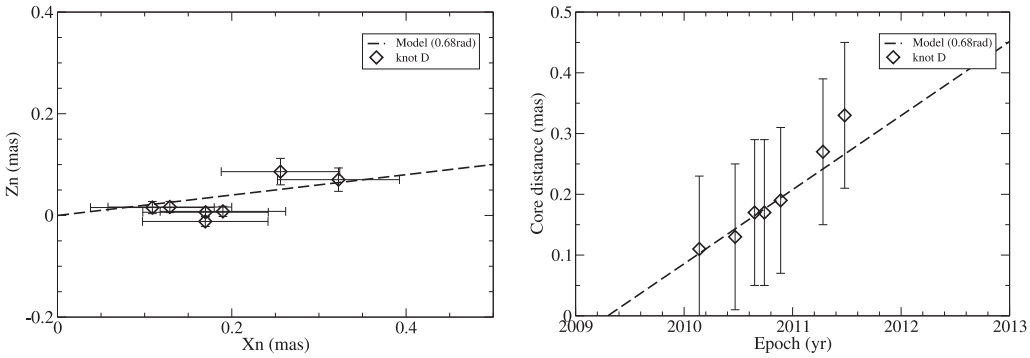

Fig. 23 Fitting to the trajectory and core distance of knot D. Ejection time $t_0 = 2009.30$.

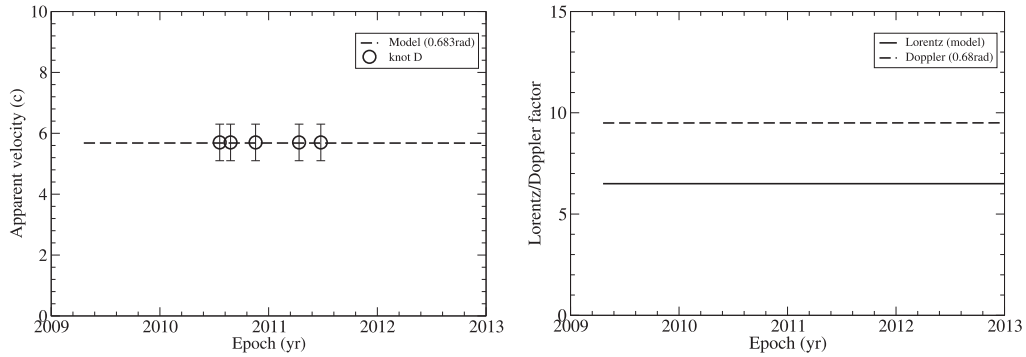

Fig. 24 Fitting of the apparent velocity and the Lorentz/Doppler factor derived from the model for knot D.

(2) Essentially, our model describes a precessing nozzle: the combination of a sequence of isolated (individual) components ejected from the precessing nozzle constitutes the so called jet and its change with time seen in VLBI maps of 3C 454.3. Similar models have been suggested in

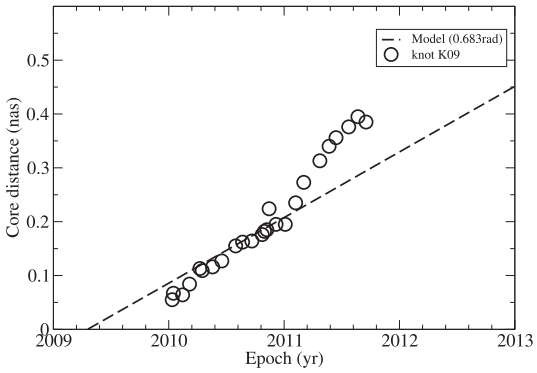

Fig. 25 Fitting to the core distance of K09 detected at 43 GHz by Jorstad et al. (2012). The precession model gives a good fit the first part of its trajectory (before 2011), which is fully consistent with the fit to the trajectory of knot D observed at 15 GHz (Britzen et al. 2013; see Fig. 23).

Tateyama & Kingham (2004, OJ287)[2], Stirling et al. (2003, BL Lac), Tateyama (2009, BL Lac), Jorstad et al. (2005). Much earlier, the precessing ballistic model suggested by Hjellming & Johnston (1981, radio jet) and Margon et al. (1980, optical jet) for SS 433 showed that individual components were ejected by the precessing nozzle (or core) at different ejection angles and then moved along a ballistic trajectory. By contrast, in the case of 3C 454.3, the individual knots ejected from the precessing nozzle seem to interact with the surrounding interstellar medium (forming shocks) and 'sweep out' a 'cavity-like' structure close to the central engine (with an arc-structure at its boundary detected by Britzen et al. 2013). Due to the effect of projection at a small viewing angle in the case of 3C 454.3, this 'cavity-like' structure is particularly prominent. The relativistic plasma flowing in the cavity appears to converge at distances of $X_n \gtrsim 3$ mas and be re-ejected as an 'ordinary' jet (see Fig. 26 (left)). This behavior is very similar to that suggested by Blandford & Rees (1974) in their twin-exhaust model (or beam model) for the formation of extended double sources. Certainly, the knots and associated plasma should be tightly wound by helical magnetic fields (e.g., Camenzind 1990; Vlahakis & Königl 2004).

Thus in the case of 3C 454.3, we see a new mechanism for large-scale jet formation: a jet on the scale of parsecs is formed by the precessing nozzle which is produced by a black-hole-accretion disk system and then the jet plasma, spanning parsecs, re-converges and is re-ejected from the 'cavity' by a 'second nozzle,' forming a large-scale jet. This process may also occur in other blazars.

(3) In Figure 27 is shown the modeled distribution of the precession phase of the superluminal components (left panel) and the modeled distribution of their ejection position angle (right panel). It can be seen that our fits span more than two periods of precession (from ∼1979 to 2010).

The modeled relationship between the viewing angle of the ejection and its position angle is shown in Figure 28 (left). It can be seen that the viewing angles derived for the knots are in the range $\sim 1^\circ$ to 5°. The bulk Lorentz factors determined from the fitting are shown in Figure 28 (right). The derived Lorentz factors are in the range 4 to 15, and they show no regular trend. Thus the different apparent speeds observed for different knots could not be explained in terms of only

[2] Agudo et al. (2012) recently suggested that at 7 mm the swing of the position angle for the jet position in blazar OJ 287 is erratic, which is different from the regular (precession) behavior at cm wavelengths during the period of 1995–2004 studied by Tateyama & Kingham (2004) and supported by Moór et al. (2011). This difference still needs to be investigated further. Here we only discuss the models of a precessing nozzle.

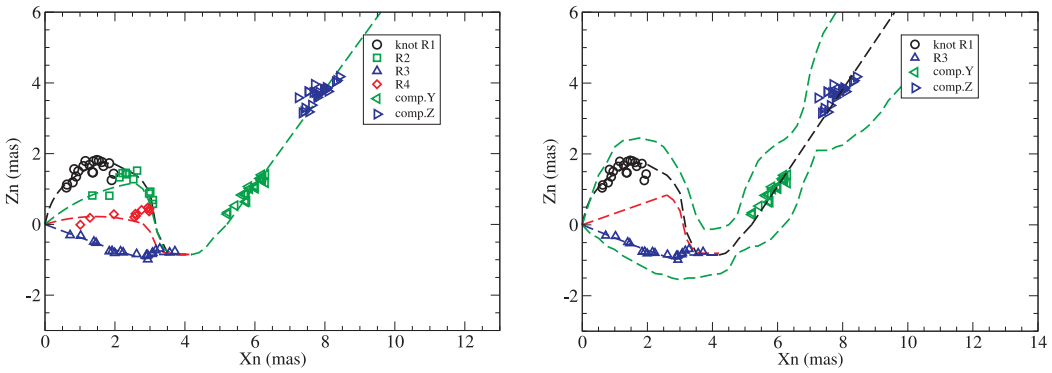

Fig. 26 A conceptual sketch illustrating the convergence of trajectories for the superluminal components and the formation of the ring structure detected in Britzen et al. (2013). *Left*: convergence of the trajectories for the superluminal components and their convergence onto the axis of the jet where components Y and Z are located. Dashed lines indicate the trajectory of knots R1 (*black*), R2 (*green*), R4 (*red*) and R3 (*blue*) (referring to Fig. 2). *Right*: shape of the jet when sizes of components are taken into account. The green dashed lines indicate the jet boundaries defined by the sizes of superluminal knots. The red dashed line within $X_n = 2.5$ mas of the core denotes the projected precession axis. Note: the sharp curvatures of the trajectories (X_n <3 mas) are largely magnified by the projection effects at small viewing angles.

a change in viewing angle with a constant Lorentz factor. The bulk Lorentz factor of the knots could be mainly determined by the activity of the engine (black hole/accretion disk system). This conclusion is consistent with what was derived from the study of kinematics observed with VLBI in blazar 3C 279 (Qian 2013). In addition, we point out that for alternative precession models with smaller values of parameter ϵ, larger bulk Lorentz/Doppler factors would be obtained.

We point out that our precession scenario is tentative and can only explain the kinematics of part of the superluminal components. In fact, The phenomena observed with VLBI in blazar 3C 454.3 are exceptionally complex, as shown by Britzen et al. (2013). The kinematic behavior (initial ejection, trajectory and ejection velocity etc.) of the components can be affected by several different physical mechanisms and precession is only one of them. Further studies are needed to reveal if precession is a significant factor governing the kinematic behavior of superluminal components.

Based on this study, we found that a few other factors should perhaps be considered, for example, formation of both stationary and traveling components/shocks. Very small apparent speeds observed in the initial portions of the trajectory of knots A and B detected by Britzen et al. (2013) might alternatively be due to the formation of quasi-stationary shocks or re-confinement shocks (Daly & Marscher 1988; Sikora et al. 2008). Thus, the precession model proposed in this paper may be used as a guide to further study the kinematic behavior of superluminal components in 3C 454.3 and disentangle different factors and mechanisms, especially for those superluminal components which could not be accommodated into our precession model.

5 MECHANISMS CAUSING PRECESSION OF THE JET NOZZLE

If the jet precession with a period of about 14.5 yr (rest-frame period $14.49/(1+z) = 7.8$ yr) is plausible, then precession of the jet nozzle might be directly related to the formation of the jet, because the swing in the ejection position angle of the knots is independent of their apparent superluminal motion.

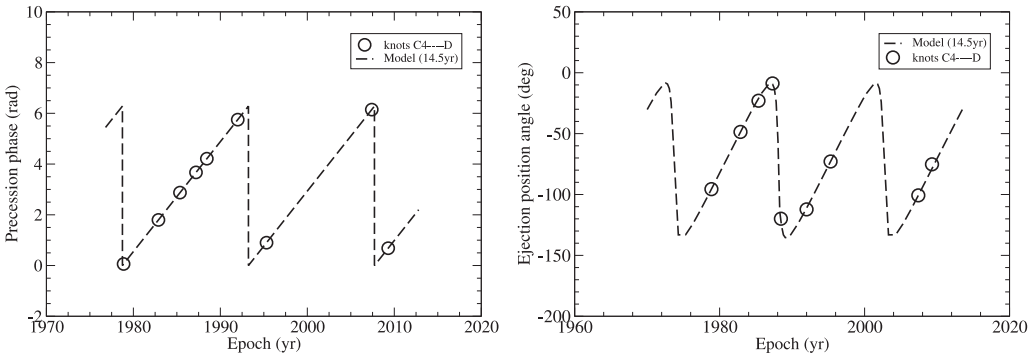

Fig. 27 *Left*: Modeled distribution of the precession phase of the knots. *Right*: Modeled distribution of the ejection position angle; Points represent knots C4, R1, R2, R3, R4, A, B, C and D.

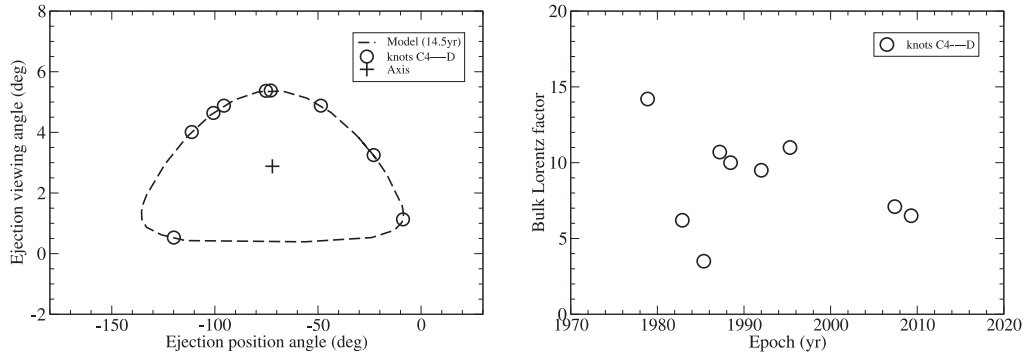

Fig. 28 *Left*: Modeled relation between ejection viewing angle and ejection position angle. The plus symbol indicates the position of the precession axis; *Right*: bulk Lorentz factors derived from the fitting; Points represent knots C4, R1, R2, R3, R4, A, B, C and D.

5.1 Formation of Jets

Relativistic jets are suggested to be formed in the rotating magnetosphere above a black hole's event horizon, ergosphere and inner disk (Meier et al. 2001; Meier & Nakamura 2006). Three mechanisms have been proposed:

(1) Hole-driven mechanism (Blandford/Znajek mechanism) (Blandford & Znajek 1977; MacDonald & Thorne 1982): jets are formed by extraction of energy from the spinning black hole (Kerr hole) and the magnetic fields are anchored to the event horizon. Jets are presumed to be oriented along the spin axis of the Kerr black hole;
(2) Ergosphere-driven mechanism (e.g., Punsly 1996, 2011; Metzler et al. 1999; Meier 1999; Meier et al. 2001; Meier & Nakamura 2006; Punsly & Coroniti 1990): Jets are formed by extraction of energy from the spinning black hole through the differential frame-dragging of space around the rapidly spinning hole within the ergosphere. The magnetic fields of the jets are anchored in the ergospheric disk. Jets are presumed to be oriented along the spinning axis of the Kerr black hole.

(3) Accretion disk-driven mechanism (e.g. Blandford & Payne 1982; Camenzind 1990): Jets are formed in the disk magnetosphere by extraction of energy from the differential rotation of the disk. The magnetic fields are anchored in the inner disk (outside the ergosphere). Jets are presumed to be oriented along the axis of the rotating disk around the spinning black hole.

These mechanisms may be all at work in blazars and give jets a stratified structure. In fact, jets in blazars are often observed to have a spine-sheath structure: hole-driven and/or ergosphere-driven relativistic plasma flows that give rise to gamma ray jets form a spine and the disk-driven flows form radio jets as a sheath. The relativistic electrons emitting radiation at a different energy bands are accelerated in different strata of jets and the associated magnetic fields could have different structures in different strata.

5.2 Possible Mechanisms for Jet Precession

Several mechanisms have been proposed to interpret swings in the position angle of jets observed in blazars. For example, the helically twisted jet model (Hardee 1987; Denn et al. 2000; Tateyama et al. 1998, 2002), precessing helical jet model and precessing ballistic (nozzle) model (Tateyama & Kingham 2004). For interpretation of precession in a jet nozzle, two mechanisms may be relevant: the binary black hole model (e.g. Begelman et al. 1980; Tateyama & Kingham 2004) and the Lense-Thirring effect (Liu & Melia 2002; Britzen et al. 2001; Caproni et al. 2004).

5.2.1 Binary black hole model

A binary black hole model (precessing disk model) was first proposed by Begelman et al. (1980) and has been extensively investigated by, e.g. Roos et al. (1993); Katz (1997); Britzen et al. (2001); Lobanov & Roland (2005); Karouzos et al. (2010). In binary black hole models, the orbital motion of a companion black hole can cause precession of the accretion disk around the primary black hole by dynamic torque, if the disk is inclined relative to the orbital plane, leading to precession of the jet that is anchored to the disk.

This kind of model has been applied by Lobanov & Roland (2005; for 3C 345) and Britzen et al. (2001; for PKS1420–140) to interpret optical variations (light curves) and properties of their parsec-scale jet. However, in binary black hole models, orbital periods are usually in the range of a few hundred years and the periods of precession reach thousands of years. Such periods of precession seem too long to explain precession in the jet nozzle obtained for 3C 454.3, because the period of precession of 14.5 yr derived in this paper is independent of any effects of relativistic time shortening. In fact, binary black-hole mechanisms have been suggested to interpret the precession of large-scale jets (kpc–Mpc scales, for example, see Gower et al. 1982).

Valtonen & Wiik (2012) applied a binary black hole model to interpret the 12 yr period in the optical light curves of OJ 287. In their model, the passage of the companion black hole crossing the disk of the primary hole was assumed to cause the periodicity[3]. They have also discussed the variation of position angle for the parsec scale radio jet. However, it is not clear if this model could be applied to interpret the swing in the ejection position angle of the superluminal components in the case of 3C 454.3, because in their model the variation of the position angle in a parsec scale jet was delayed by a few years with respect to the companion black hole passing across the disk of the primary black hole.

[3] In Valtonen & Wiik (2012) the observed period of 12 yr was explained in terms of the orbital period of the companion black hole.

5.2.2 Lense-Thirring effect

The Lense-Thirring effect has been suggested to cause disk precession and could be a promising mechanism for explaining the jet/nozzle precession with a time scale of years. (Lense & Thirring 1918; Bardeen & Petterson 1975; Liu & Melia 2002; Caproni et al. 2004).

The Lense-Thirring effect shows that under the influence of strong gravity of a spinning (Kerr) black hole, its accretion disk would be precessed by inertial-frame dragging if the disk is inclined to the equatorial plane of the spinning black hole[4]. At small radii in the disk, the differential Lense-Thirring precession will dominate internal coupling of the plasma and will lead to the so called Bardeen-Petterson effect, in which the inner region flattens toward the equatorial plane, producing a warped accretion disk. Regions in the outer disk would retain their rotation axis which is misaligned with the spin axis of the black hole. Thus the structure of an accretion disk around a rapidly rotating black hole has a warped structure that could be divided into three distinct regions: inner region, transition region and outer region. The inner region is closest to the Kerr black hole and its axis of rotation is aligned with the spin axis of the hole. The outer region could still keep its original direction of rotation inclined to the spin axis and have nothing to do with the jet precession. The transition region might be relevant for understanding precession in the jet nozzle observed in blazars, because in the transition zone the disk regions would still be misaligned with respect to the equatorial plane of the spinning black hole. Thus the axis of a jet (jet nozzle) with its base anchored to the transition regions of the disk would precess around the spin axis of the black hole with small opening angles. As shown by Scheuer (1992), for a maximally rotating black hole with mass $10^8 - 10^9\,M_\odot$, a Lense-Thirring period of precession on the order of years is obtainable for an accretion radius of 10–100 Schwarzschild radii ($R_{\rm s}$).

Nelson & Papaloizou (2000) have investigated the transition of alignment between the accretion disk and Kerr black hole by hydromagnetic simulations of the Bardeen-Petterson effect in various conditions. They showed that the transition radius was found to be much smaller than that given by Bardeen & Petterson (1975, $10^2 - 10^4\,R_{\rm g}$), ranging between 15 and 30 $R_{\rm g}$ ($R_{\rm g}$ is gravitational radius, $R_{\rm g} = R_{\rm s}/2$) for a hole with a Kerr angular momentum parameter $a_* = 1$ (maximal spin of the black hole). This range is quite similar to the observed size of the jet's base in radio galaxy M87 (see below).

Recently, a 'magneto-spin alignment' mechanism has been proposed for thick disks to study the alignment between disks/jets and Kerr black holes (McKinney et al. 2013; Tchekhovskoy et al. 2011) and revealed that electro-magnetic torque exerted by the magnetized jet, which is directly generated by the rotating black hole, on a tilted disk can cause magnetized disks and jets to align with the spin of a nearby black hole and ones further away to reorient with the outer disk.

Therefore, theoretical studies have shown that the Lense-Thirring effect plus internal disk viscosity and electromagnetism could cause misalignment between the rotation axis of the disk and the spin axis of a Kerr black hole, and precession of a jet around the axis of the black hole.

5.3 Observational Constraints

Theoretical models of jet formation predict quite a large range of size for the jet's base, which depends on the size of the region where the jet is initially accelerated and the twisted magnetic fields are anchored. In disk-driven jet formation models (e.g. Blandford & Payne 1982; Camenzind 1990), the rotating magnetic fields are anchored to the inner part of the rotating accretion disk; the

[4] Sarazin et al. (1980) proposed that the black hole and inner disk could be precessed by the outer disk via the Lense-Thirring effect, if the accretion disk is sufficiently massive and its total angular momentum significantly exceeds that of the black hole. However, this mechanism gives very long precession periods ($10^4 - 10^7$ yr), only applicable to large scale jet structures in radio galaxies and radio quasars (Lu 1990).

jet plasma is accelerated to relativistic speeds and collimated outside the light cylinder (Camenzind & Krockenberger 1992) with its foot-point radius near the inner last stable orbit around a rapidly rotating black hole. The radius of the light cylinder is about $R_{\rm L} \sim 10\,R_{\rm g}$, but the cylindrical radius of the jet's base where collimation occurs is estimated to be $\sim 5-50\,R_{\rm L}$ ($\sim 50-500\,R_{\rm g}$). Superluminal knots are assumed to be ejected near this jet's base.

In formation models for an ergospheric disk-driven and hole-driven jet (e.g. Punsly & Coroniti 1990; Blandford & Znajek 1977), the size of the jet's base may be much smaller than that given by models for a disk-driven jet, which might be less than $20-30\,R_{\rm g}$.

However, the magnetohydrodynamic theory of jet formation indicates (e.g., Camenzind 1990) that jet formation occurs in a family of magnetic surfaces that have a stratified structure. Radiation at different frequencies could be emitted by different magnetic surfaces, with higher frequency emission coming from inner strata and lower frequency emission from outer strata.

Recent high-resolution VLBI observations at millimeter wavelengths for radio galaxy M87 (one of the nearest giant elliptical galaxies) have obtained important information about the structure of the jet and the size of the jet's base. Observations at 7 mm by Ly et al. (2007) showed edge-brightened emission of the jet and a wide opening angle at its core. The 86 GHz (λ3.5 mm) VLBI observations by Krichbaum et al. (2006) showed that the size of the core (jet nozzle), as observed with VLBI, was less than $30\,R_{\rm g}$. Recent 230 GHz (λ1.3 mm) VLBI observations of the jet associated with radio galaxy M87 (Doeleman et al. 2012) have shown that the size of its jet's base is only $\sim 5.5\,R_{\rm s}$ (or $11\,R_{\rm g}$), and the 43 GHz (λ7 mm) VLBI observations by Hada et al. (2011, 2012) have shown that the bright compact core observed at 7 mm (i.e. the jet's base) is located within $14-23\,R_{\rm s}$ ($28-46\,R_{\rm g}$) of the supermassive black hole (mass $\simeq 6.4\times10^9\,M_\odot$; Gebhardt & Thomas 2009; Gebhardt et al. 2011). The size of the core observed with VLBI has been measured to be $\sim 34\,R_{\rm g}$, suggesting that the jet associated with M87 is powered by the innermost part of an accretion disk (in a prograde orbit) around a spinning black hole.

Moreover, VLBI observations at 1.3 mm (Doeleman et al. 2012), 3.5 mm (Krichbaum et al. 2006) and 7 mm (Hada et al. 2011) revealed that the width of the jet's base follows a power law as a function of distance from the origin of the jet (Asada & Nakamura 2012). Thus the inferred width of the core at 2 cm is $\sim 54\,R_{\rm g}$. (Note: this is the size of a Gaussian fit to the core, but its full size should be $\sim 100\,R_{\rm g}$).

5.4 A Possible Estimation of Black Hole Spin in 3C 454.3

If the Lense-Thirring effect is a plausible interpretation for precession of the jet in 3C 454.3, then we can relate the period of precession to the spin of the black hole.

According to Liu & Melia (2002) and assuming that the surface mass density of the disk is independent of the disk radius and its inner radius is much larger than the gravitational radius, the Lense-Thirring driven period of precession can be approximately written as

$$P_{\rm obs}({\rm yr}) = (1+z)3.5\frac{M_9}{a_*}\,\bar{r}_{\rm out}^{\frac{5}{2}}\,\bar{r}_{\rm in}^{\frac{1}{2}}\,, \tag{8}$$

where M_9 is the mass of the spinning supermassive black hole in units of 10^9 solar masses, a_* is the dimensionless specific angular momentum (spin parameter) ($= J/J_{\rm max}$, $J_{\rm max} = GM^2/c$, $0 \le a_* \le 1$, and J is the spin angular momentum of the black hole. $\bar{r}_{\rm out} = r_{\rm out}/60\,R_{\rm g}$, $\bar{r}_{\rm in} = r_{\rm in}/6\,R_{\rm g}$. Here $r_{\rm out}$ and $r_{\rm in}$ are the outer and inner radii of the transition region of the accretion disk on which the precession jet is assumed to be anchored. In the case of 3C 454.3, the half opening angle of the precession cone is $\simeq 2.5^\circ$ (see Sect. 2). Such a small inclination angle of the inner disk with respect to the equatorial plane of the black hole might be possible, before it is forced to be fully aligned with the axis of the spinning black hole by the strong gravitational torque.

Both theoretical studies and observations with VLBI predict that the transition region might have a range of radius of $10 - 100\,R_{\rm g}$ (see Sects. 5.3 and 5.4), if we assume $\bar{r}_{\rm out} = 1$, $\bar{r}_{\rm in} = 1$ and $P_{\rm obs} = 14.5$ yr. Thus we obtain the ratio between the mass and the spin of the black hole in 3C 454.3 as ($z = 0.859$)

$$\frac{M_9}{a_*} \simeq 2.2\,. \tag{9}$$

The mass of the black hole in 3C 454.3 has been measured. For $M_{\rm BH} \sim 1.6 \times 10^9\ M_\odot$ (Woo & Urry 2002) $a_* \sim 0.73$. But for $M_{\rm BH} \sim 4.4 \times 10^9\ M_\odot$ (Gu et al. 2001), there is no solution for a_*. In this case the dependence of the surface mass density on the disk radius may need to be taken into account and an appropriate set of parameters (a_*, M_9, $\bar{r}_{\rm out}$ and $\bar{r}_{\rm in}$) could be found to fit the period of precession (Caproni et al. 2004). Therefore a spin-induced precession (or the Lense-Thirring effect) could be a feasible mechanism driving the precession of the nozzle. In addition, if the precessing region of the disk is closer to the black hole than that assumed above, then the Lense-Thirring period would become shorter. In that case, we would have to take into account the increase in the period of precession from the foot points in the disk to the jet's base (and jet nozzle).

6 CONCLUSIONS

In this paper, we have discussed fits to the model of the kinematics describing nine superluminal components in blazar 3C 454.3. It has been shown that a scenario for precession in the jet nozzle might explain their kinematic behavior in a unified way. Obviously, the model is oversimplified and, strictly speaking, the obtained period of precession of 14.5 yr is a quasi-period. We have shown that the kinematics of the jet are fitted well by a model that has a precessing nozzle in which a single precession axis, amplitude function and period of precession are common to all eject from the jet. The proposed model is only tentative and inconclusive. The precession model itself cannot decide whether precession of the jet really exists or not. Future VLBI observations in two or more cycles (20–30 yr) can test the model, checking whether superluminal components are ejected at the predicted position angles. We have found that a few knots cannot be accommodated in this precession model and other (additional) mechanisms or factors need to be explored (e.g., instabilities in the magnetic surface structure (e.g. erratic variation or jump in the orientation of the jet)). However, our model seems to be useful for studying the physical mechanisms of kinematics of the knots in 3C 454.3 and helpful for disentangling different factors or mechanisms associated with behaviors of different knots. In a separate paper, we will discuss the interpretation of the kinematics of some of the components observed at other frequencies, e.g., by Jorstad et al. (2001, 2005, 2010, 2012).

Acknowledgements We thank the anonymous referee for the constructive comments and suggestions which were most helpful for improving the paper.

References

Abdo, A. A., Ackermann, M., Agudo, I., et al. 2010, ApJ, 716, 30
Abdo, A. A., Ackermann, M., Ajello, M., et al. 2009, ApJ, 699, 817
Abdo, A. A., Ackermann, M., Ajello, M., et al. 2011, ApJ, 733, L26
Agudo, I. 2009, in ASPC, 402, Approaching Micro-Arcsecond Resolution with VSOP-2: Astrophysics and Technologies, eds. Y. Hagiwara, E. Fomalont, M. Tsuboi, & M. Yasuhiro, 330
Agudo, I., Gómez, J.-L., Martí, J.-M., et al. 2001, ApJ, 549, L183
Agudo, I., Bach, U., Krichbaum, T. P., et al. 2007, A&A, 476, L17
Agudo, I., Jorstad, S. G., Marscher, A. P., et al. 2011, ApJ, 726, L13
Agudo, I., Marscher, A. P., Jorstad, S. G., et al. 2012, ApJ, 747, 63

Asada, K., & Nakamura, M. 2012, ApJ, 745, L28
Bach, U., Krichbaum, T. P., Ros, E., et al. 2005, A&A, 433, 815
Bardeen, J. M., & Petterson, J. A. 1975, ApJ, 195, L65
Begelman, M. C., Blandford, R. D., & Rees, M. J. 1980, Nature, 287, 307
Blandford, R. D., & Rees, M. J. 1974, MNRAS, 169, 395
Blandford, R. D., & Znajek, R. L. 1977, MNRAS, 179, 433
Blandford, R. D., & Payne, D. G. 1982, MNRAS, 199, 883
Bonning, E. W., Bailyn, C., Urry, C. M., et al. 2009, ApJ, 697, L81
Bonnoli, G., Ghisellini, G., Foschini, L., Tavecchio, F., & Ghirlanda, G. 2011, MNRAS, 410, 368
Britzen, S., Roland, J., Laskar, J., et al. 2001, A&A, 374, 784
Britzen, S., Witzel, A., Gong, B. P., et al. 2010, A&A, 515, A105
Britzen, S., Qian, S. J., Witzel, A., et al. 2013, A&A, 557A, 37
Camenzind, M. 1990, Accretion and Winds, in: Reviews in Modern Astronomy, ed. G. Klare, 234 (Berlin: Springer-Verlag)
Camenzind, M., & Krockenberger, M. 1992, A&A, 255, 59
Caproni, A., Mosquera Cuesta, H. J., & Abraham, Z. 2004, ApJ, 616, L99
Chatterjee, R., Jorstad, S. G., Marscher, A. P., et al. 2008, ApJ, 689, 79
Daly, R. A., & Marscher, A. P. 1988, ApJ, 334, 539
Denn, G. R., Mutel, R. L., & Marscher, A. P. 2000, ApJS, 129, 61
Doeleman, S. S., Fish, V. L., Schenck, D. E., et al. 2012, Science, 338, 355
Donnarumma, I., Pucella, G., Vittorini, V., et al. 2009, ApJ, 707, 1115
Finke, J. D., & Dermer, C. D. 2010, ApJ, 714, L303
Foschini, L., Ghisellini, G., Tavecchio, F., Bonnoli, G., & Stamerra, A. 2011, A&A, 530, A77
Fuhrmann, L., Cucchiara, A., Marchili, N., et al. 2006, A&A, 445, L1
Gebhardt, K., Adams, J., Richstone, D., et al. 2011, ApJ, 729, 119
Gebhardt, K., & Thomas, J. 2009, ApJ, 700, 1690
Ghisellini, G., Foschini, L., Tavecchio, F., & Pian, E. 2007, MNRAS, 382, L82
Giommi, P., Blustin, A. J., Capalbi, M., et al. 2006, A&A, 456, 911
Gomez, J. L., Marti, J. M. A., Marscher, A. P., Ibanez, J. M. A., & Alberdi, A. 1997, ApJ, 482, L33
Gower, A. C., Gregory, P. C., Unruh, W. G., & Hutchings, J. B. 1982, ApJ, 262, 478
Gu, M., Cao, X., & Jiang, D. R. 2001, MNRAS, 327, 1111
Hada, K., Doi, A., Kino, M., et al. 2011, Nature, 477, 185
Hada, K., Kino, M., Nagai, H., et al. 2012, ApJ, 760, 52
Hardee, P. E. 1987, ApJ, 318, 78
Hjellming, R. M., & Johnston, K. J. 1981, ApJ, 246, L141
Hogg, D. W. 1999, astro-ph/9905116
Jorstad, S. G., Marscher, A. P., Mattox, J. R., et al. 2001, ApJS, 134, 181
Jorstad, S. G., Marscher, A. P., Lister, M. L., et al. 2005, AJ, 130, 1418
Jorstad, S. G., Marscher, A. P., Stevens, J. A., et al. 2007, AJ, 134, 799
Jorstad, S. G., Marscher, A. P., Larionov, V. M., et al. 2010, ApJ, 715, 362
Jorstad, S., Marscher, A., Smith, P., et al. 2012, International Journal of Modern Physics Conference Series, 8, 356 (arXiv:1111.0110)
Karouzos, M., Britzen, S., Eckart, A., Witzel, A., & Zensus, A. 2010, A&A, 519, A62
Katz, J. I. 1997, ApJ, 478, 527
Krichbaum, T. P., Graham, D. A., Bremer, M., et al. 2006, Journal of Physics Conference Series, 54, 328 (astro-ph/0607072)
Kudryavtseva, N. A., Britzen, S., Witzel, A., et al. 2011, A&A, 526, A51
Kudryavtseva, N. A., & Pyatunina, T. B. 2006, Astronomy Reports, 50, 1

Lense, J., & Thirring, H. 1918, Phys.Z. 19, 156
Liu, S., & Melia, F. 2002, ApJ, 573, L23
Lobanov, A. P., & Roland, J. 2005, A&A, 431, 831
Lu, J. F. 1990, A&A, 229, 424
Lu, R.-S., Fish, V. L., Akiyama, K., et al. 2013, ApJ, 772, 13
Ly, C., Walker, R. C., & Junor, W. 2007, ApJ, 660, 200
MacDonald, D., & Thorne, K. S. 1982, MNRAS, 198, 345
Margon, B., Grandi, S. A., & Downes, R. A. 1980, ApJ, 241, 306
Marscher, A. P. 2008, in ASPC, 386, Extragalactic Jets: Theory and Observation from Radio to Gamma Ray, eds. T. A. Rector, & D. S. De Young, 437
Marscher, A. P., & Jorstad, S. G. 2011, ApJ, 729, 26
Marscher, A. P., Jorstad, S. G., Agudo, I., MacDonald, N. R., & Scott, T. L. 2012, arXiv:1204.6707
McKinney, J. C., Tchekhovskoy, A., & Blandford, R. D. 2013, Science, 339, 49
Meier, D. L. 1999, ApJ, 522, 753
Meier, D. L., Koide, S., & Uchida, Y. 2001, Science, 291, 84
Meier, D. L., & Nakamura, M. 2006, in ASPC, 350, Blazar Variability Workshop II: Entering the GLAST Era, eds. H. R. Miller, K. Marshall, J. R. Webb, & M. F. Aller, 195
Metzler, C. A., White, M., Norman, M., & Loken, C. 1999, ApJ, 520, L9
Moór, A., Frey, S., Lambert, S. B., Titov, O. A., & Bakos, J. 2011, AJ, 141, 178
Nelson, R. P., & Papaloizou, J. C. B. 2000, MNRAS, 315, 570
Pacciani, L., Vittorini, V., Tavani, M., et al. 2010, ApJ, 716, L170
Pauliny-Toth, I. I. K. 1998, in IAU Colloq. 164: Radio Emission from Galactic and Extragalactic Compact Sources, ASPC, 144, eds. J. A. Zensus, G. B. Taylor, & J. M. Wrobel, 75
Pauliny-Toth, I. I. K., Porcas, R. W., Zensus, J. A., et al. 1987, Nature, 328, 778
Pen, U.-L. 1999, ApJS, 120, 49
Pian, E., Foschini, L., Beckmann, V., et al. 2006, A&A, 449, L21
Punsly, B. 1996, ApJ, 473, 178
Punsly, B. 2011, MNRAS, 418, L138
Punsly, B., & Coroniti, F. V. 1990, ApJ, 350, 518
Qian, S.-J. 2011, RAA (Research in Astronomy and Astrophysics), 11, 43
Qian, S.-J. 2012, RAA (Research in Astronomy and Astrophysics), 12, 46
Qian, S.-J. 2013, RAA (Research in Astronomy and Astrophysics), 13, 783
Qian, S. J., Witzel, A., Krichbaum, T., et al. 1991, Acta Astron. Sin. 32, 369 (English translation: in Chin. Astro. Astrophys. 16, 137)
Qian, S.-J., Kudryavtseva, N. A., Britzen, S., et al. 2007, ChJAA (Chin. J. Astron. Astrophys.), 7, 364
Qian, S.-J., Witzel, A., Zensus, J. A., et al. 2009, RAA (Research in Astronomy and Astrophysics), 9, 137
Raiteri, C. M., Villata, M., Aller, M. F., et al. 2011, A&A, 534, A87
Raiteri, C. M., Villata, M., Bruschini, L., et al. 2010, A&A, 524, A43
Raiteri, C. M., Villata, M., Larionov, V. M., et al. 2008, A&A, 491, 755
Roos, N., Kaastra, J. S., & Hummel, C. A. 1993, ApJ, 409, 130
Sarazin, C. L., Begelman, M. C., & Hatchett, S. P. 1980, ApJ, 238, L129
Savolainen, T., Wiik, K., Valtaoja, E., & Tornikoski, M. 2006, A&A, 446, 71
Scheuer, P. A. G. 1992, in Extragalactic Radio Sources. From Beams to Jets, eds. J. Roland, H. Sol, & G. Pelletier, 368
Sikora, M., Moderski, R., & Madejski, G. M. 2008, ApJ, 675, 71
Spergel, D. N., Verde, L., Peiris, H. V., et al. 2003, ApJS, 148, 175
Stirling, A. M., Cawthorne, T. V., Stevens, J. A., et al. 2003, MNRAS, 341, 405
Striani, E., Vercellone, S., Tavani, M., et al. 2010, ApJ, 718, 455

Tateyama, C. E. 2009, ApJ, 705, 877
Tateyama, C. E., & Kingham, K. A. 2004, ApJ, 608, 149
Tateyama, C. E., Kingham, K. A., Kaufmann, P., et al. 1998, ApJ, 500, 810
Tateyama, C. E., Kingham, K. A., Kaufmann, P., & de Lucena, A. M. P. 2002, ApJ, 573, 496
Tchekhovskoy, A., Narayan, R., & McKinney, J. C. 2011, MNRAS, 418, L79
Tosti, G. 2007, in AIPC, 921, The First GLAST Symposium, eds. S. Ritz, P. Michelson, & C. A. Meegan, 255
Valtonen, M. J., & Wiik, K. 2012, MNRAS, 421, 1861
Vercellone, S., Chen, A. W., Giuliani, A., et al. 2008, ApJ, 676, L13
Vercellone, S., Chen, A. W., Vittorini, V., et al. 2009, ApJ, 690, 1018
Vercellone, S., D'Ammando, F., Vittorini, V., et al. 2010, ApJ, 712, 405
Vercellone, S., Striani, E., Vittorini, V., et al. 2011, ApJ, 736, L38
Vercellone, S. 2011 (arXiv1111.0697)
Villata, M., Raiteri, C. M., Balonek, T. J., et al. 2006, A&A, 453, 817
Villata, M., Raiteri, C. M., Aller, M. F., et al. 2007, A&A, 464, L5
Vlahakis, N., & Königl, A. 2004, ApJ, 605, 656
Woo, J.-H., & Urry, C. M. 2002, ApJ, 579, 530